International Journal of Machine Tools and Manufacture 123 (2017) 146–159

Contents lists available at ScienceDirect

International Journal of Machine Tools and Manufacture

journal homepage: www.elsevier.com/locate/ijmactool

Flow behavior of powder particles in layering process of selective laser melting: Numerical modeling and experimental verification based on discrete element method

Hui Chen, Qingsong Wei *, Shifeng Wen, Zhongwei Li, Yusheng Shi

State Key Laboratory of Materials Processing and Die & Mould Technology, School of Materials Science and Engineering, Huazhong University of Science and Technology, Wuhan, 430074, PR China

ARTICLE INFO

Keywords:
Powder layering
Particle flow
Selective laser melting
Additive manufacturing
Discrete element method

ABSTRACT

Powder-layering is an essential process of selective laser melting (SLM), but the underlying mechanisms of powder movement and packing at particle scale is unclear. Based on discrete element method (DEM), this study proposed a numerical model to investigate the flowing behavior of powder layered by a blade, where the contact force and cohesion force between individual particles were considered. DEM simulations gave visual morphologies of the flow profiles and velocity fields for powder-layering at particle scale, as well as the relationships between the quality of powder bed and the layering parameters. The model was validated by experiment results in terms of the macroscopic profiles of powder during layering, showing good prediction accuracy. Then, dynamic repose angle (DRA) and mass flow rate (MFR) were defined to make quantitative evaluation on the powder flow. Preliminary research shows that, the powder fluidity increases with the decreasing of particle friction coefficients, resulting in a denser and more uniform powder bed. The decreasing of particle radius R over the range of $R > 21.8$ μm can benefit the powder fluidity. However, when the particle radius decreases in the range of $R < 21.8$ μm, the weight of cohesion force rises and thus makes the powder fluidity worse. The increase of layering speed enhances the dilation of moving particles, and the decrease of layering height intensifies the local force-arches in particles. These will reduce the continuity and stability of the powder flow and is unfavorable for improving the density or uniformity of the layered powder bed.

1. Introduction

Selective Laser Melting (SLM), as a powder-based additive manufacturing process, has become an important technology for the production of a wide variety of components and structures in the last decade [1]. It is a powder-bed fusion process that employs high intensity laser as an energy source to melt and fuse selective regions of powder materials, layer by layer, basing on computer aided design (CAD) date. As depicted in Fig. 1a, the SLM consists of two major processing steps in each fabrication period [2,3]: powder-layering and powder-melting. Firstly, in the step of powder-layering, the delivery chamber rises by a certain level, and the building chamber declines with one layer thickness. Then the powder in delivery chamber is scraped into the building chamber by a layering apparatus to form a layer of powder bed. Secondly, in the step of powder-melting, a high energy density laser is used to melt selected areas of the powder bed, according to the CAD data. These two processing steps are repeated for successive layers of powder until the required part is completely built. The quality of the fabricated part is mainly influenced by three aspects [4]: the scan strategy of laser, the material formulation of powder, and the state of the powder bed. So far, an overwhelming majority of investigations are focused on the scan strategy of laser and the material formulation of powder in order to improve the quality of the fabricated part [5]. Actually, as shown in Fig. 1b, the state of the powder bed formed in powder-layering, such as packing density and homogeneity, will make great affection on the laser heat transfer within it, and thus change the macro performance of the fabricated parts.

General conclusion is that a loose powder bed with cavity or shifting defects will make the powder-melting worse and then induce melt defects such as balling, pore or denudation which decrease the macro quality of final parts, while powder bed with dense and uniform state is desirable for SLM. With numerical methods, for instance, Gutler et al. [6]

* Corresponding author. School of Materials Science and Engineering, Huazhong University of Science and Technology, Luoyu Street 1037, Wuhan, 430074, PR China.
E-mail address: wqs_xn@163.com (Q. Wei).

http://dx.doi.org/10.1016/j.ijmachtools.2017.08.004
Received 15 July 2017; Received in revised form 27 August 2017; Accepted 29 August 2017
Available online 1 September 2017

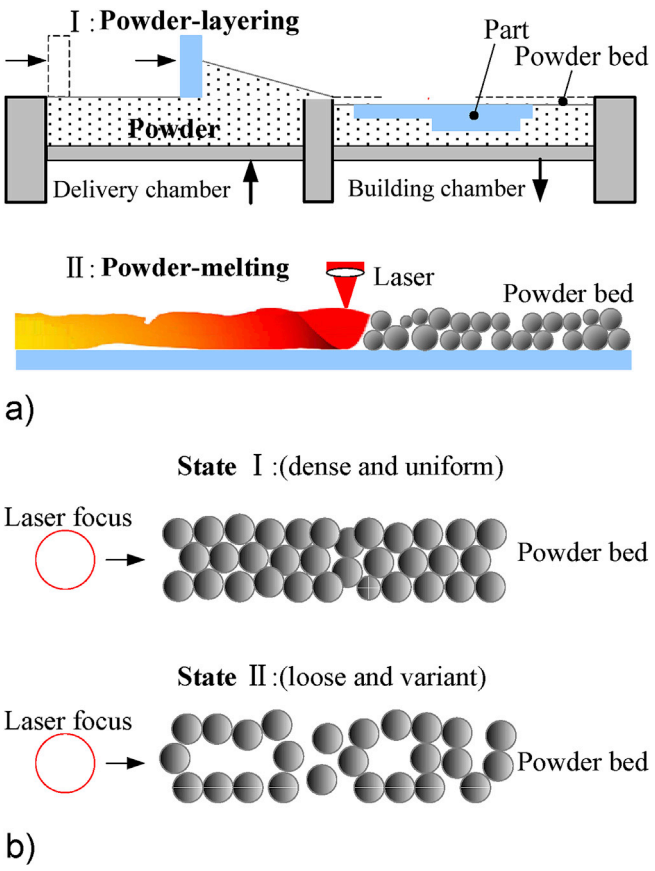

Fig. 1. Schematic of: (a) two major processing steps of SLM; and (b) the state of the layered powder bed.

employed the computer fluid dynamic (CFD) method and were the first to show a 3D model of powder melting and solidification, where the arrangement of powder bed at particle scale was considered. Lee and Zhang [7] made a study similar to Gutler et al. and emphasized the importance of particle size distribution. They pointed out that balling defects in SLM was a manifestation of melting instability and added that a higher packing density of powder bed could decrease the effect. Khairallah et al. [3,8] reported a highly resolved model with Finite Element Method (FEM) which considered a powder bed of 316L stainless steel with a size distribution. They found that the laser heat transfer fluctuated more violently in loosely packed powder bed with cavities, which would break up the track of molten pool and hence induce melt defects such as balling and pores. And similar conclusion was also obtained in the study of Xia et al. [1], where CFD model was employed to evaluate the pore evolution of randomly packed powder bed. Experimental research about this issue is in rare number and limited to qualitative analysis. Ziegelmeier et al. in Ref. [9] proposed that the surface quality and porosity of the fabricated part were highly dependent on the packing density and roughness of the layered powder bed. Recently, Matthews et al. [10] made a direct observation about the evolution of melt pool in powder bed, using high-speed camera and microscope. They emphasized various zones of the powder bed and proposed that the densely packed powder could decrease the denudation size around the melt pool and hence reduce the generation of pores. These numerical and experimental researches show the significant connection between the part fabricating and the state of powder bed at particle scale. However, the powder-layering, as the processing step determining the state of powder bed, are not linked to almost all these studies. Therefore, these results can not be directly used for optimizing the process parameters to improve the quality of fabricated parts in SLM. To address this issue, it is necessary to investigate the processing step of powder-layering and clarify the forming mechanism of the powder bed first.

The powder bed layered in SLM is a typical kind of solid particle system, presenting a characteristic of spatial and temporal varying fashion at particulate scale [11]. The state of the powder bed, such as packing density, uniformity and layer defects, are directly resulted from the powder-layering and determined by the flowing mechanism of individual particles [12]. The flow mechanism of the powder during layering is extremely complex, due to the random and discontinuous nature of particle motion. All factors such as physical properties of particle, cohesion force between particles, and contact status between particles and layering apparatus can affect the flowing of the powder, and thus change the state of the powder bed. Some researchers pay their attention to the processing step of powder-layering and try to improve the macroscopic quality of the layered powder bed. For example, Marchelli et al. [13] declared that the thickness of each layered powder bed should be greater than the largest particles due to the issue of powder spreadability. Lu and Reynolds [14] conducted the powder-layering by counter rolling method and found that, in case of layering thin powder bed, it was prone to cause layering defects such as cavities which would degrade the integrities of the powder bed. And they attributed this problem to the existence of cohesion force in powder such as Van der Waals' force. In the work of Cao et al. [15], a double-smoothing method was proposed on their self-developed machine to layer ultra-thin powder bed, and the cavity-type defects were effectively eliminated in their observations. Xiang et al. [16] simplified the layering process by considering a direct assembly of particles and found that the packing density of powder bed increases with the layer thickness. Until now, there have been hardly any reports on the flow mechanism of powder-layering at particulate scale, and the factors affecting the forming of the powder bed are not clear, even for the spherical powder particles layered by the simplest layering apparatus.

The materials commonly used in SLM manufacturing are metal powder which is fine and opaque, so there is an unavoidable difficulty in experimental measuring the flow information of powder-layering at particle scale, such as particle velocities or particle trajectories. Then, an attractive alternative to answering this challenge is through modeling and predictive simulations. Currently, the numerical techniques commonly employed in the studies of SLM, such as FEM [3,8] and CFD [1,6] mentioned above, are based on the continuous medium theory. Due to the discrete nature of powder material, both the FEM and CFD are insufficient to describe its physical process, especially for the powder-layering where complex mechanical mechanisms between individual particles exist. Then the numerical technique based on the discrete media theory, such as discrete element method (DEM) originally proposed by Cundall and Strack [17], is undoubtedly the best option. The DEM based on Newton's law of motion is capable of describing the dynamic behavior of discontinuous material systems. A great deal of researches using DEM technique have already been found in the geomechanics and rock mechanics literature, owing to this method's usefulness in problems of brittle fracture [18]. Other common DEM applications are in the studies of granule processing such as mixing in rotating drum [19], grinding in ball mill [20], granulating in pelletizer [21] and discharging in hopper [22–24]. This technique has already proven efficient in providing insight into dynamics phenomena occurring in particulate system. The detailed flowing information of all individual particles such as velocity, position, trajectory and contact force, which are difficult to acquire by experiments alone, can be evaluated conveniently as well as the macroscopic packing state of particles [25–27]. Recently, Parteli and Pöschel [28] developed a DEM model for the first time to simulate preliminarily the process of powder-layering in a quasi-2D condition, presenting the potential of DEM in the investigation of the flowing and packing behavior of powder particles in SLM. However, lots of fundamental work still needs to deal with. For instance, how to validate the numerical model experimentally, how to characterize quantitatively the flow behavior powder during layering which determines the state of the powder bed, and so on.

The objective of this study is to reveal the flowing behavior of the

powder during layering at particle scale, and make understanding about the forming mechanism of the powder bed in SLM manufacturing. To do so, a three-dimensional DEM model was developed to simulate the powder-layering process. The powder was restricted to the spherical particles, and the layering apparatus considered here was a relatively simple blade. The interaction forces and cohesion forces between powder particles were considered and embedded into the model. The DEM model was validated by experiment results in terms of the profiles of the powder pile during layering, using image processing method. Then the dynamic repose angle (DRA) and mass flow rate (MFR) of the powder were defined to make quantitatively characterization of its flowing behavior, which will determine the packing density and uniformity of the powder bed. The effects of material properties of particles, cohesion force between particles, and processing parameters of layering apparatus on the powder flowing were investigated.

2. Methods

2.1. Condition of powder-layering for simulation and experiment

There are two main kinds of powder-layering methods in SLM: scraping and counter-rolling [15]. The scraping method is relatively simple and commonly used in industrial machines (such as EOS, SLM Solution and Renishaw), as it just needs a blade [13]. So, it was considered as the powder-layering form in this study.

Fig. 2a sketched the physical model of powder-layering for DEM simulations and physical experiments, where L and W are the length and width of the layering zone, respectively; H is the layering height, defined as the distance between the surface of the part and the bottom of the blade. A layering starts with the random packing of powder particles in delivery chamber, where the surface of the packed powder is $2H$ higher than the bottom of the blade. Next, the blade moves along the X direction with a constant speed, i.e., the layering speed $\boldsymbol{V}$, to collect he powder and feed it onto the surface of part in building chamber. The blade stops moving until a layer of powder bed is spread on the part. Then, one cycle of powder-layering is completed. Note that a moving coordinate O′-X′Y′Z′ fixed on the blade was employed for the convenience of flow analysis. In order to validate the numerical model, the 1: 1 scale physical experiments were conducted under similar conditions. Note that the wall of experimental device in the XZ plane was made of polymer Plexiglas to allow for optical observations, and then the process of powder-layering was followed by a video camera perpendicularly to the XZ plane.

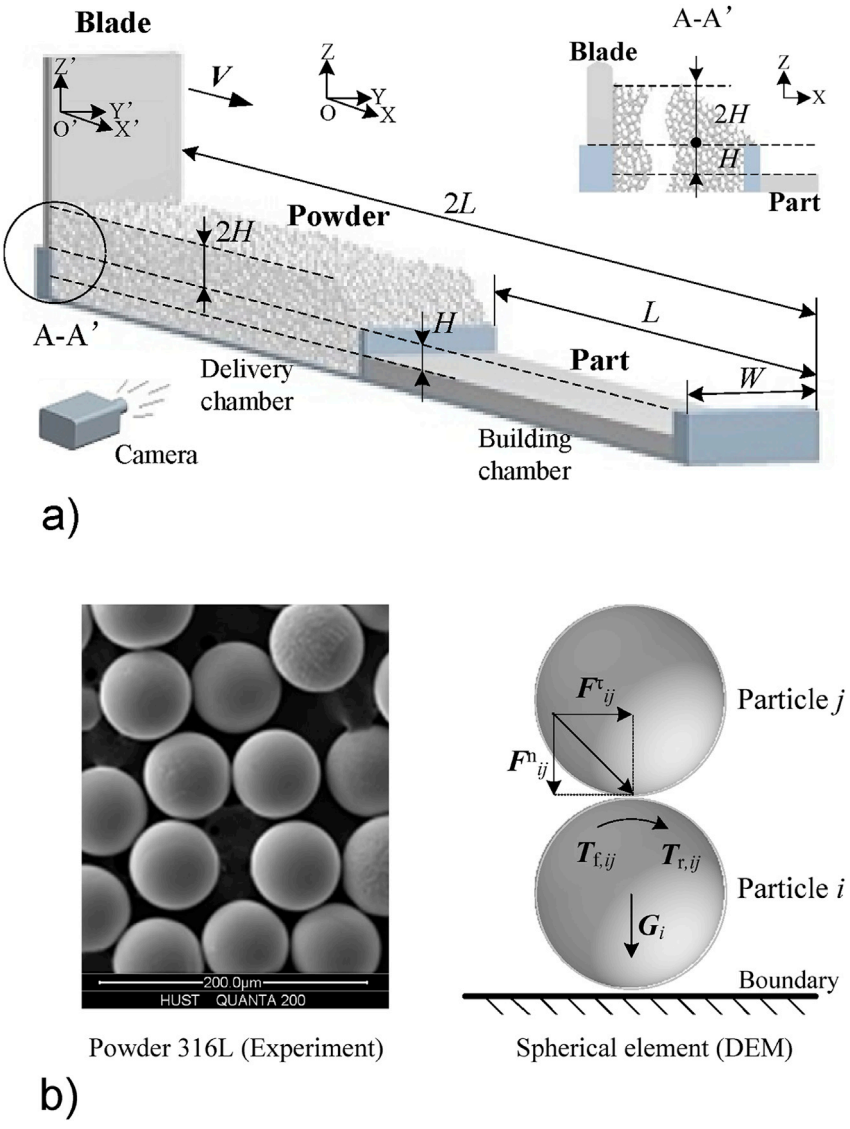

Fig. 2. Schematic of powder-layering condition for simulation and experiment: (a) initial state of powder-layering; and (b) powder represented by spherical element.

The powder system constituted of non-spherical particles behaves differently from the one composed of spherical particles, as the relative motion between particles will be restricted to some extent due to the particle irregular [31]. However, most kinds of metal powder used in SLM are actually spherical particles [1,5,8], although small shape error exists. And this is indeed the case for the 316L powder employed in our powder-layering experiments, as shown in Fig. 2b. Therefore, the effect of particle shape on the powder flow was not considered currently, and the spherical element was used to represent the powder particles in DEM simulations. For one of the particle i, as shown in Fig. 2b, the total forces acting on it include gravity as well as interaction forces accounting for the particle/particle and particle/boundary interactions. The total torque on particle i is the summation of all forces with respect to it. In this study, the interaction of particle/boundary is of the same constitutive model as particle/particle interaction. Note that the geometry boundaries (the blade and part) are considered as special particles whose mass is infinitely large, and hence the motion of geometry boundaries is not affected by the powder particles.

2.2. DEM modeling

2.2.1. Governing equations

As the particle system in powder-layering belongs to dense particle flow regime, the three-dimensional DEM technique with "soft-sphere approach [17,29]" was employed. The motion of each individual powder particle, during the layering, can be described by Newton's second law of motion. As shown in Fig. 2b, the translational and rotational motions of particle i in the system at time t, caused by its interactions with neighboring particle j or boundaries, can be described by the following equations:

$$m_i\frac{\mathrm{d}\mathbf{u}_i}{\mathrm{d}t} = \mathbf{G}_i + \sum_j\left(\mathbf{F}^{\mathrm{n}}_{ij} + \mathbf{F}^{\tau}_{ij}\right) \tag{1}$$

$$I_i\frac{\mathrm{d}\boldsymbol{\omega}_i}{\mathrm{d}t} = \sum_j\left(\mathbf{T}_{\mathrm{f},ij} + \mathbf{T}_{\mathrm{r},ij}\right) \tag{2}$$

where m_i, I_i, $\boldsymbol{u}_i$, and $\boldsymbol{w}_i$ are, respectively, the mass, moment of inertia, translational velocity, and rotational velocity of particle i; $\boldsymbol{G}_i$ is the gravitational force of particle i. $\boldsymbol{F}^{\mathrm{n}}_{ij}$ and $\boldsymbol{F}^{\tau}_{ij}$ are, respectively, the normal and tangential interaction forces between particle i and j. The normal and tangential interaction forces are respectively composed of contact fore and damping force, i.e., $\boldsymbol{F}^{\mathrm{n}}_{ij} = \boldsymbol{F}^{\mathrm{n}}{}_{\mathrm{c},ij} + \boldsymbol{F}^{\mathrm{n}}{}_{\mathrm{d},ij}$, and $\boldsymbol{F}^{\tau}_{ij} = \boldsymbol{F}^{\tau}{}_{\mathrm{c},ij} + \boldsymbol{F}^{\tau}{}_{\mathrm{d},ij}$. Then the simplified Hertz-Mindlin contact force model proposed by Tsuji et al. [32], which makes a reasonably precise representation of the particle moving behavior during collisions without increasing too amounts of computational costs [33], is employed to figure the damping forces ($\boldsymbol{F}^{\mathrm{n}}{}_{\mathrm{d},ij}$ and $\boldsymbol{F}^{\tau}{}_{\mathrm{d},ij}$) and tangential contact force forces $\boldsymbol{F}^{\tau}{}_{\mathrm{c},ij}$ due to the particle deformations. And these interaction forces are summed over the particles j being in contact with particle i. $\boldsymbol{T}_{\mathrm{f},ij}$ is the torque generated by tangential components of contact forces which cause particle i to rotate, and $\boldsymbol{T}_{\mathrm{r},ij}$ is the rolling friction torque that opposes to the rotation of particle i. All the details of forces and torques involved in the translational and rotational motion equations of particle i are summarized in Table 1. Note that the normal contact force $\boldsymbol{F}^{\mathrm{n}}{}_{\mathrm{c},ij}$, taking into account the component of cohesion force, will be described below.

Cohesion forces between particulate materials make great effects on the collision and moving behaviors of particles. For dry metal powder particles at micron scale, there is no need to consider the cohesion forces such as liquid bridge force and electrostatic force. However, the considerable Van der Waals force is unavoidable and prone to cause layering defects during the layering of fine powder [11,13,15]. Therefore, in addition to contact force due to particle deformation, the Van der Waals force must be taken into account in our DEM program. Following the JKR theory [34], the Van der Waals force is implanted into the normal contact force $\boldsymbol{F}^{\mathrm{n}}{}_{\mathrm{c},ij}$ through modifying the Hertz-Mindlin contact model [32] by introducing additional attractive force between particles. Then, $\boldsymbol{F}^{\mathrm{n}}{}_{\mathrm{c},ij}$ depends on the surface energy density of particle, γ, in the following way:

Table 1
List of equations to calculate various kinds of forces and torque acting on particle i.

Forces and torques		Symbols	Equations
Normal direction	Interaction force	$\mathbf{F}^{\mathrm{n}}_{ij}$	$\mathbf{F}^{\mathrm{n}}_{ij} = \mathbf{F}^{\mathrm{n}}_{\mathrm{c},ij} + \mathbf{F}^{\mathrm{n}}_{\mathrm{d},ij}$
	Contact force	$\mathbf{F}^{\mathrm{n}}_{\mathrm{c},ij}$ [34,35]	$F^{\mathrm{n}}_{\mathrm{c},ij} = -4\sqrt{\pi\gamma E^*}r^{\frac{3}{2}} + \frac{4E^*}{3R^*}r^3$, $r^4 - 2R^*\delta^{\mathrm{n}}r^2 - \frac{4\pi\gamma}{E^*}R^{*2}r + R^{*2}\delta^{\mathrm{n}2} = 0$
	Damping force	$\mathbf{F}^{\mathrm{n}}_{\mathrm{d},ij}$ [32]	$F^{\mathrm{n}}_{\mathrm{d},ij} = -\sqrt{\frac{20}{3}}\beta\left[E^*m^*(R^*\delta^{\mathrm{n}})^{\frac{1}{2}}\right]^{\frac{1}{2}}u^{\mathrm{n}}_{ij}$
Tangential direction	Interaction force	$\mathbf{F}^{\tau}_{ij}$	$\mathbf{F}^{\tau}_{ij} = \mathbf{F}^{\tau}_{\mathrm{c},ij} + \mathbf{F}^{\tau}_{\mathrm{d},ij}$
	Contact force	$\mathbf{F}^{\tau}_{\mathrm{c},ij}$ [32]	$F^{\tau}_{\mathrm{c},ij} = -\min\{F_{\mathrm{f}}, \left\|8G^*\sqrt{R^*\delta^{\mathrm{n}}}\delta^{\mathrm{t}}\right\|\}$
	Damping force	$\mathbf{F}^{\tau}_{\mathrm{d},ij}$ [32]	$F^{\tau}_{\mathrm{d},ij} = \sqrt{\frac{80}{3}}\beta(G^*\sqrt{R^*\delta^{\mathrm{n}}}m^*)^{\frac{1}{2}}u^{\mathrm{t}}_{ij}$
Friction force		$\mathbf{F}_{\mathrm{f}}$	$F_{\mathrm{f}} = \mu_{\mathrm{s}}\left\|\mathbf{F}^{\mathrm{n}}_{\mathrm{c},ij}\right\|$
Friction torque		$\mathbf{T}_{\mathrm{f},ij}$	$\mathbf{T}_{\mathrm{f},ij} = \mathbf{R}_i \times \mathbf{F}^{\tau}_{\mathrm{c},ij}$
Rolling torque		$\mathbf{T}_{\mathrm{r},ij}$	$\mathbf{T}_{\mathrm{r},ij} = -\mu_{\mathrm{r}}R_i\mathbf{F}^{\mathrm{n}}_{\mathrm{c},ij}\widehat{\boldsymbol{\omega}}_i$
Gravitational force		$\mathbf{G}_i$	$\mathbf{G}_i = m_i\mathbf{g} = \frac{4}{3}\pi R_i^3\rho i\mathbf{g}$

Where the equivalent properties in terms of the properties of particle i and j are respectively $R^* = R_iR_j/(R_i+R_j)$, $m^* = m_im_j/(m_i+m_j)$, $E^* = E_iE_j/[(1\text{-}\xi_j^2)E_i+(1\text{-}\xi_i^2)E_j]$, and $G^* = G_iG_j/[(1\text{-}\xi_j)G_i+(1\text{-}\xi_i)G_j]$; the transform coefficient is $\beta = \ln e/(\ln^2 e + \pi^2)^{0.5}$; the unit angular velocity is $\widehat{\boldsymbol{\omega}}_i = \boldsymbol{\omega}_i/|\boldsymbol{\omega}_i|$; R_i, E_i, G_i, ξ_i and R_i, E_i, G_i, ξ_i are respectively the radius, Young's modulus, shear modulus, and Poisson ratio of particle i and j; γ, μ_{s}, μ_{r}, and e are respectively the surface energy, sliding friction coefficient, rolling friction coefficient, and restitution coefficient between particle i and j; $\boldsymbol{u}^{\mathrm{n}}_{ij}$ and $\boldsymbol{u}^{\tau}_{ij}$ stand for, respectively, the normal and tangential relative velocities between particle i and j when a collision occurs (where: $\mathbf{n} = \mathbf{R}_i/|\mathbf{R}_i|$, $\boldsymbol{u}^{\mathrm{n}}_{ij} = (\boldsymbol{u}_i\text{-}\boldsymbol{u}_j)\cdot\mathbf{n}$, and $\boldsymbol{u}^{\tau}_{ij} = (\boldsymbol{u}_i\text{-}\boldsymbol{u}_j + \boldsymbol{R}_i\times\boldsymbol{\omega}_i + \boldsymbol{R}_j\times\boldsymbol{\omega}_i)\times\mathbf{n}$); then δ^{n} and δ^{τ} signify, respectively, the normal and tangential overlaps between particle i and j during the collision and can be obtained through the integration of $\boldsymbol{u}^{\mathrm{n}}_{ij}$ and $\boldsymbol{u}^{\tau}_{ij}$; ρ_i is the density of particle i; and $\boldsymbol{g}$ is the gravitational acceleration.

$$F^{\mathrm{n}}_{\mathrm{c},ij} = -4\left(\pi E^*\gamma\right)^{\frac{1}{2}}r^{\frac{3}{2}} + \frac{4E^*}{3R^*}r^3 \tag{3}$$

where the intermediate variable r is the contact spot radius between particle i and j, related to the normal overlap δ^{n} through the equation [35]:

$$r^4 - 2R^*\delta^{\mathrm{n}}r^2 - \frac{4\pi\gamma}{E^*}R^{*2}r + R^{*2}\delta^{\mathrm{n}2} = 0 \tag{4}$$

According to Eqs. (3) and (4), non-zero attractive force still exists, even though particles are not in contact with each other (i.e., $\delta^{\mathrm{n}} < 0$). Then a critical value of distance between particles, $\delta^{\mathrm{n}}_{\mathrm{c}}$, is employed in this work for the calculating of normal contact force $F^{\mathrm{n}}{}_{\mathrm{c},ij}$, which is given by Ref. [36]:

$$\delta^{\mathrm{n}}_{\mathrm{c}} = \frac{r_{\mathrm{c}}^2}{R^*} - \sqrt{\frac{4\pi\gamma r_{\mathrm{c}}}{E^*}},\quad r_{\mathrm{c}} = \frac{9\left(3\sqrt{2}-4\right)\pi\gamma R^{*2}}{8\sqrt{2}E^*} \tag{5}$$

Note that the value of $\delta^{\mathrm{n}}_{\mathrm{c}}$ is always less than zero in Eq. (5). When the distance between particles exceeds the critical value, i.e., $\delta^{\mathrm{n}} < \delta^{\mathrm{n}}_{\mathrm{c}}$, the value of zero returns to the normal contact force $F^{\mathrm{n}}{}_{\mathrm{c},ij}$, and the application of program module for calculating $F^{\mathrm{n}}{}_{\mathrm{c},ij}$ in our DEM model will not be considered in order to decrease the computational costs.

When the distance between non-contacting particles is small than the critical value, i.e., $\delta^{\mathrm{n}}_{\mathrm{c}} < \delta^{\mathrm{n}} < 0$, the maximum cohesion force between particles due to the Van der Waals force, known as the "pull-out force [34,36]", F_{pullout}, can be obtained by maximizing the absolute value of $F^{\mathrm{n}}{}_{\mathrm{c},ij}$ in Eq. (3), which is given by:

$$F_{\text{pullout}} = \max\left|F^{\text{n}}_{\text{c},ij}\right| = \frac{3}{2}\pi R^{*}\gamma \tag{6}$$

In this study, we specify the strength of the cohesion force in terms of a dimensionless parameter K, which is defined as the ratio of the pull-out force to the weight of individual powder particle:

$$K = \frac{F_{\text{pullout}}}{G_i} = \frac{3\pi R\gamma}{2m_i g} = \frac{9\gamma}{8\rho_i g R^2} \tag{7}$$

The parameter K here is called the "bonding-number" and used to specify how strong the attraction between individual particles is. Then, the larger the bounding-number, the stronger the attraction between particles is. According to Eq. (7), the bounding-number K is proportional to the surface energy density γ but inversely proportional to the square of the particle radius R^2.

Besides, for the case without Van der Waals force, i.e., $\gamma = 0$, the normal contact force $\boldsymbol{F}^{\text{n}}_{\text{c},ij}$ in Eq. (3) turns into the Hertz normal contact force [32], which is given by:

$$F^{\text{n}}_{\text{c},ij|_{\gamma=0}} = F_{\text{hertz}} = \frac{4}{3}E^{*}R^{*\frac{1}{2}}\delta^{\text{n}\frac{3}{2}} \tag{8}$$

This is the sole repulsive elastic component of the normal contact force between individual particles. In the calculation of interaction forces in tangential direction, the contact force $\boldsymbol{F}^{\tau}_{\text{c},ij}$ (see Table 1) is bounded by the friction force F_{f}, following the Coulomb law of friction. Similar to the tangential force implementation discussed by Gilabert et al. [36], the normal contact force in the form of Eq. (8) is applied to calculate the friction force in this DEM program, i.e., $F_{\text{f}} = \mu_{\text{s}}\left|\mathbf{F}^{\text{n}}_{\text{c},ij}\right| = \mu_{\text{s}}\left|F^{\text{n}}_{\text{c},ij|_{\gamma=0}}\right|$.

2.2.2. Time step

The time step Δt for calculating the incremental contact forces and displacements of particles should be smaller than the characteristic time Δt_{c}. Then, the Rayleigh critical time step [20], a typical characteristic time, was employed for Δt_{c}:

$$\Delta t_c = \pi\left[\frac{R_i}{0.163\xi_i + 0.877}\sqrt{\frac{2\rho_i(1+\xi_i)}{E_i}}\right]_{\min} \tag{9}$$

Choosing a suitable time step for the DEM program is generally a trade-off between the computation cost, the calculation error, and the stability of the integration scheme. As O'Sullivan and Bray [37] reported, the reasonable time step Δt for the simulation of dense particles' movement varied between 20% and 80% of Rayleigh critical time step. In this work, considering both of the computation cost and accuracy, the value of 50% of Δt_{c} was chosen to calculate the governing equations of this model.

2.2.3. DEM parameters

The base values of particle properties were specified to the ones of 316L powder (Fig. 2b) which was sieved into different particle sizes and employed in experiments. Strictly speaking, all parameters of particle in DEM model should be set the same as those in corresponding experiment for the model validation. However, the Young's modulus of particle in numerical model was two orders of magnitude less than the real value, in order to increase the time step for calculation (see Eq. (9)), making the long computation of DEM code more bearable. Actually, it is a general way using a Young's modulus lower than its true value to reduce the computation costs in DEM technique [38], as the sensitivity of numerical results is ignorable for a wide value range of the Young's modulus [25]. The restitution coefficient between particles was the empirical value directly obtained from the literature [39]. Rolling friction coefficient between particles is difficult to measure. As the rolling resistance between hard spheres such as steel or glass particles is extremely week, it is common in DEM simulations that the rolling friction coefficient is assumed to be very small or even ignored [19–21], and acceptable results can be obtained by these treatments. Therefore, considering that the steel powder used in our experiments was of spherical shape, the base value of rolling friction coefficient between particles was set to a small value of 0.01.

The base values of sliding friction coefficient μ_{s} and surface energy density γ for the particles were calibrated in our trial simulations, where the macroscopic flow profile of the powder during layering was compared between the numerical and experimental results. Both the sliding friction coefficient and surface energy density can affect the macroscopic flow profile of the powder. However, for powder with size larger than 100 μm, the effect of Van der Vals force between particles (i.e., the γ) is very week and can be ignored [15,34,35], and the friction force becomes the only factor. So, in comparing the flow profile of the powder with size larger than 100 μm from the experiments and simulations, we removed the module of cohesion force in the DEM model and found that the DEM results with $\mu_{\text{s}} = 0.61$ could agree relatively well with the experimental ones. Then, the surface energy density γ was calibrated by comparing the simulations and experiments for powder with size smaller than 100 μm, and we observed that the numerical results with the assumption of $\gamma = 0.097$ mJ/m^2 could fit relatively well with the experiments. Therefore, the base values of μ_{s} and γ for particle in the DEM model were, respectively, determined as 0.61 and 0.097 mJ/m^2.

In this study, the variables affecting the flow behavior of powder during layering were categorized into three groups: the cohesion force, particle properties (the particle radius and friction coefficients) and processing conditions (the layering speed and layering height). And wide range values of these variables were employed to evaluate their effects. Table 2 lists the base values of parameters employed in the DEM model, together with the ranges of parameter variations. For convenience, unless otherwise specified, the effect of a variable was considered within a certain range while other variables were fixed to the base values in Table 2, giving a so called base condition.

Then, the discrete element code in program C++, released from DEM-Solutions Corp., Britain [30], was used to perform the simulation. The code was run in parallel on ThinStation P900 workstation, with 32 concurrent execution threads.

2.3. Experimental procedure

It is difficult to experimentally measure the microscopic information about the powder flow, such as velocities and trajectories of individual particles. However, the macroscopic flow pattern of powder-layering can be obtained and used for comparisons. And similar to some previous literatures [30,40,41], the repose angle α, which is the maximum slope

Table 2
Base values and ranges of variables considered in the DEM model.

Name of variables	Symbol	Base value	Variable range
Particle density	ρ, kg/m^3	7.8×10^3	–
Young's modulus of particles	E, MPa	2.2×10^3	–
Poisson's ratio of particle	ξ	0.3	–
Restitution coefficient of particle/particle	e	0.9	–
Particle radius	R, μm	50	9–140
Sliding friction coefficient of particle/particle	μ_{s}	0.62	0–1.0
Rolling friction coefficient of particle/particle	μ_{r}	0.01	0–0.2
surface energy density	γ, mJ/m^2	0.097	0–17
Length of layering zone	L, mm	60	–
Width of layering zone	W	40R	–
Layering height	H	6R	2-14R
Layering speed	V, mm/s	50	25–75
Acceleration of gravity	g, m/s^2	9.8	–

angle of the powder pile during layering, was considered as the criterion for the comparison between simulations and experiments.

Firstly, the powder-layering process sketched in Fig. 2a was conducted experimentally and recorded by a digital camera at a frame rate of 30 fps with a resolution of 720 × 480 pixels. The video was converted into images signed with time serial number, using the software Fast Forward Mpeg. Fig. 3a shows one of the raw images capturing the macroscopic profile of the powder pile during layering in XZ plane at a time point t. Then, according to RGB color analysis performed by Image Processing Toolbox in MATLAB [30], the surface curve of the powder pile was acquired from the raw image through the algorithms of binarization, boundary extraction, and surface segmentation. Finally, the surface curve was fitted to a straight line according to the least square principle, and the repose angle α at time t was determined as the slope angle of the line, as shown in Fig. 3b. The image processing method was also applied to the DEM results and then the comparison between simulation and experiment can be made.

3. Result and discussion

3.1. Macroscopic flowing behavior

3.1.1. Model validation

Using variables with the base values, the process of powder-layering sketched in Fig. 2a was simulated by the DEM model. Fig. 4 shows the simulated flow patterns of the powder, where the particle velocity was determined in the global coordinate O-XYZ. As shown, we divide the process of powder-layering into two stages: the collecting stage and the layering stage. The collecting stage is the process when the blade moves in the delivery chamber. As the blade moves along the X direction, the particles with positions higher than the bottom of the blade are collected gradually, forming a powder pile. And the powder pile grows bigger and bigger with the moving blade. The layering stage starts at the time when the blade moves to the building chamber (the layering zone). In this stage, the powder pile, with the repose angle α, is scraped onto the part by the blade. Then, particles tumble down along the slope of the pile continuously and deposits on the surface of the part. The size of the powder pile becomes smaller and smaller as particles gradually lay on the part. The blade stops translating until a whole layer of powder bed is formed on the surface of the part. Apparently, the quality of the layered powder bed is determined by the layering-stage. Therefore, the study of the powder flow is focused on the layering-stage.

Fig. 5 illustrates the experimental and simulated profiles of the powder pile during layering, where the radius of the powder particles are, respectively, 84.7, 61.6, 17.4, and 12.2 μm. Note that the images were extracted when the blade moves to the position of $L/2$ of the layering zone. For all the particle samples, as shown in Fig. 5, the surface curves of the powder pile from DEM simulations agree well with the corresponding experimental results, although some local differences exist in the shape of the pile. And the fitted repose angle α in simulations accords with the corresponding experiment results, with error ratio no more than 10%. This suggests that the results from the DEM model are reliable. Deviations for the simulated profile of the powder pile will derive from some inevitable sources. For instance, it is difficult, or even impossible, to keep the local conformity of the initial packing state of the powder between the simulations and experiments, owing to the disorderly nature of the powder particles. Then, error of flowing behavior occurs to individual powder particles which move randomly during the layering. This will make local differences to the profiles of the powder pile between DEM simulation and experiments. Besides, the interaction of boundary-particle was assumed to be the same as the one of particle-particle in the DEM model. However, the actual friction between the particle and the end wall of experimental device in XZ plane might be larger than the friction between particles. Then, the effects of end wall in experiments will make the repose angle marginally larger than the simulated one. And this is indeed the case as presented in Fig. 5. Certainly, the error in the constitutive equations of contact forces employed in the DEM model itself will make deviations to the final simulation results.

In addition, it should be noted that the repose angle α, as shown in Fig. 5, varies with the particle size. The repose angle decreases with the decreasing of particle size for the samples of $R = 84.7$ and 61.6 μm, but increases with the decreasing of particle size for the samples of $R = 17.4$ and 12.2 μm. This is due to the combined action from the particle size and the cohesion force associated with it, which will be discussed detailly in Section 3.3.2.

3.1.2. Dynamic repose angle (DRA)

In SLM manufacturing, powder with good fluidity is beneficial for the layering process. The repose angle mentioned above is actually a basic property of particulate materials and often employed to characterize its fluidity, where smaller α means better fluidity [22–25]. But the repose angle α is just a transient value of the pile in quasi-static state and may be insufficient to describe the powder pile over the whole layering-stage. Fig. 6 illustrates the evolutions of the powder pile with time in the layering-stage for particles with $R = 50$ μm. As shown in Fig. 6a, the results from both the DEM simulation and experiments show that the powder pile moves with the blade and diminishes progressively in size. However, the profile shape of the powder pile is stable, with a slope angle almost constant. Then, the evolutions of the repose angle α with time t are plotted in Fig. 6b. Note that the starting time of the layering-stage is specified as $t = 0$, and the dimensionless time t_d is employed:

$$t_d = \frac{t}{t_{max}} \tag{10}$$

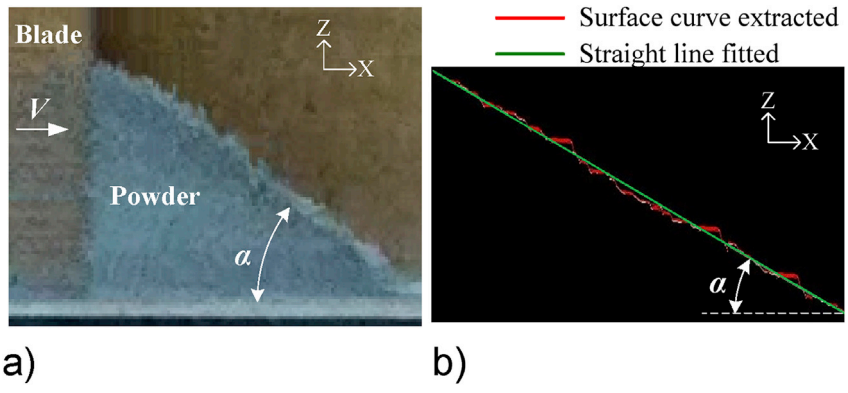

Fig. 3. Image processing to determine the repose angle α of the powder pile during layering at a time point t: (a) raw image of the powder pile; and (b) surface curve and the fitted line.

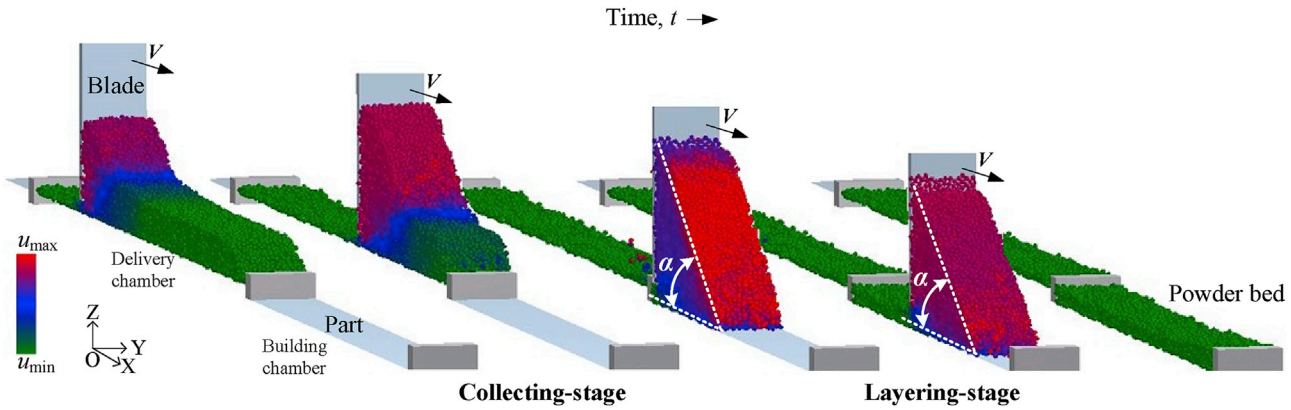

Fig. 4. Powder-layering simulated using variables with base values: flow patterns of the collecting-stage and layering-stage.

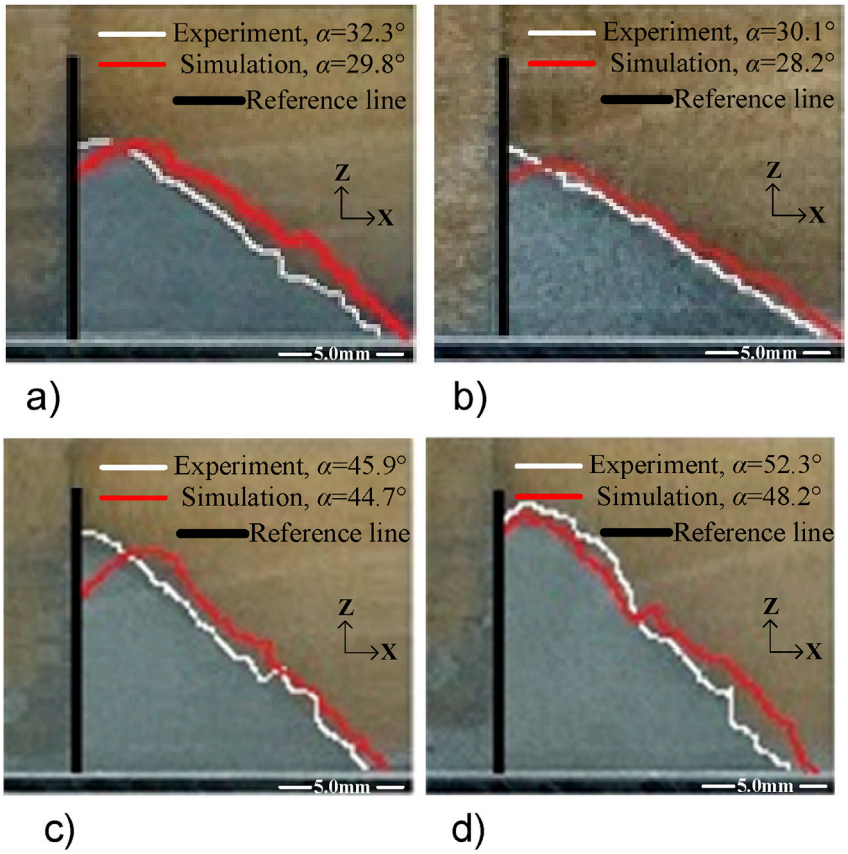

Fig. 5. Comparisons between experimental and simulated profiles of powder pile when the blade moves to the position of $L/2$ of the layering zone: (a) $R = 84.7$ μm; (b) $R = 61.6$ μm; (c) $R = 17.4$ μm; and (d) $R = 12.2$ μm.

where t_{max} is the total time spent in the layering-stage. As shown in Fig. 6b, the repose angles α of the powder piles from either simulation or experiment are almost constant during the whole process of layering-stage, although little fluctuation exists due to the random motion of particles on the surface of the pile. Then, the average value of the repose angle, $\bar{\alpha}$, is employed to characterize the fluidity of the powder in layering. And we call it the dynamic repose angle (DRA), in order to distinguish with the repose angle from the pile in quasi-static state. Similarly, smaller value of DRA means better fluidity of powder during layering.

3.2. Visualization of mass flow rate (MFR)

Flowing information at particulate scale, such as particle velocity and trajectory, is the main factor determining the state of the layered powder bed. Fig. 7a illustrates the velocity field of the powder particles when the blade moves to the middle of the layering zone (i.e., when $t_d = 0.5$), where variables with base values were used in the DEM model. Note that the particle velocity was obtained in coordinate O′-X′Y′Z′ fixed on the blade (see Fig. 2a), i.e., the velocity field is relative to the moving blade. A "shearing line" along the bottom edge of the blade and a virtual "valve" between the blade and part were added to facilitate the analysis. As shown in Fig. 7a, in the powder pile upon the shearing line can be divided

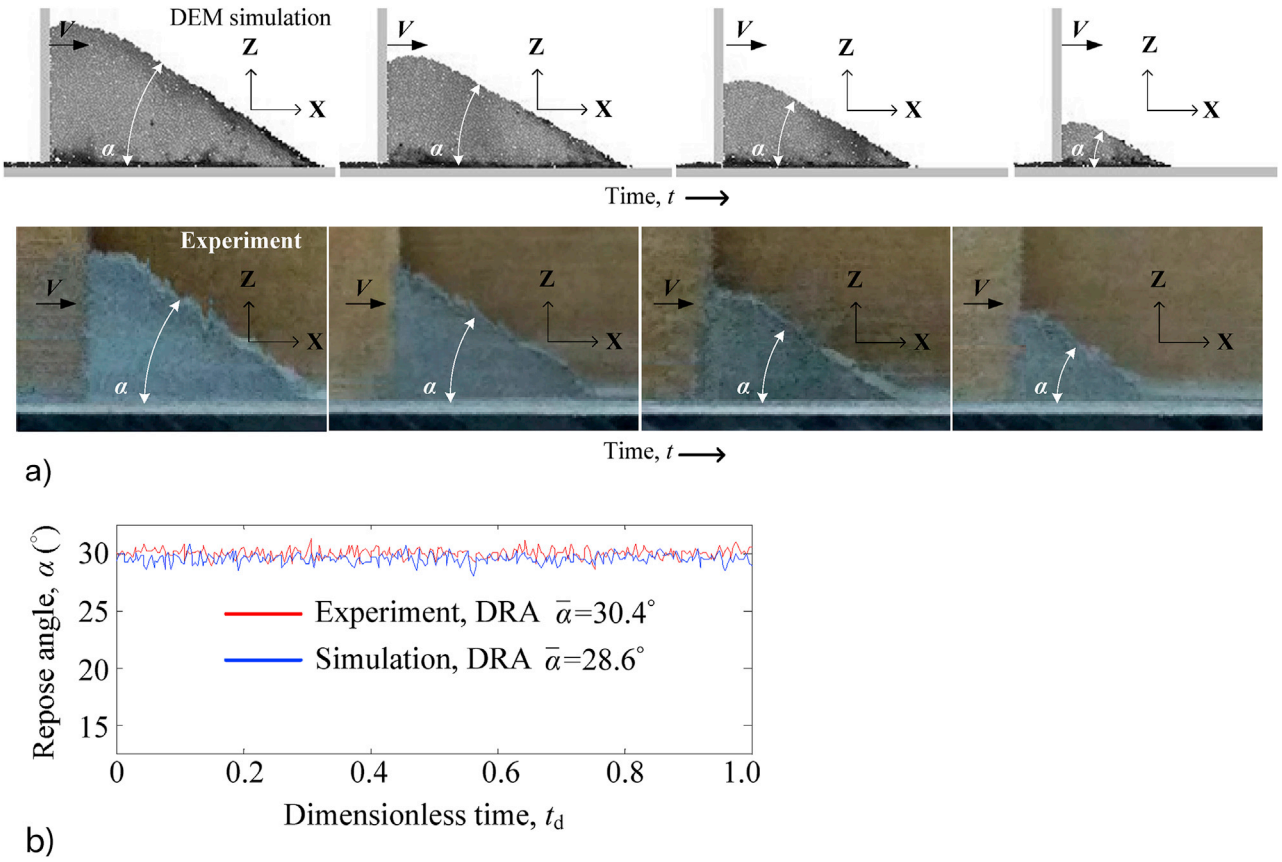

Fig. 6. Simulated and experimental results of powder pile in layering stage for $R = 50$ μm: (a) evolutions of profile of the powder pile with time t; and (b) evolutions of repose angle α with dimensionless time t_d (see Eq. (10)).

in two regions: the thin region near the slope surface where particles move down rapidly, and the rest region where particles move much slower. Then, the corresponding trajectory of powder particles plotted in Fig. 7b shows that, as particles in these two regions go through the shearing line successively, they accelerate, cross the valve, and join the powder bed. When particles have passed the valve, they reach the same speed and keep in constant, meaning that they are relatively static to each other and hence the powder bed is formed. Apparently, the quality of the powder bed is determined by the mass flow rate (MFR), q, defined as the mass of particles across the valve in unit time. For comparability, the MFR is presented in normalized form, Q, which is given by:

$$Q = \frac{q_r}{q_i} = \frac{q_r}{WHV\rho} \tag{11}$$

where q_r is the real MFR at the valve; and q_i is the ideal maximum MFR at the valve, which is calculated by $q_i = WHV\rho$ (where W, H and V are, respectively, the width of the layering zone, the layering height and the layering speed (see Fig. 2a); and ρ is the particle density). According to Eq. (11), the normalized MFR has the value range of $0 \le Q \le 1$, where larger value of Q means larger packing density of the layered powder bed. For the total layering-stage, the average value of the normalized MFR, $\overline{Q}$, will be discussed. When $\overline{Q} = 1$, it means that the whole layered powder bed gets the idea state of full density.

Moreover, the variation coefficient, Q_{vc}, is proposed to describe the stability of the particle flow at the valve, which is given by:

$$Q_{vc} = \frac{Q_{st}}{\overline{Q}} \tag{12}$$

where Q_{st} is the standard deviation of the normalized MFR for the layering stage. According to the definition of the variation coefficient Q_{vc}, smaller value of Q_{vc} means steadier particle flow at the valve, and thus more uniform powder bed can be layered. Particle flow with variation coefficient of $Q_{vc} = 0$ is the idea condition for powder-layering.

Fig. 7c plots the evolution of normalized MFR Q with dimensionless time t_d in the layering-stage, where the variables with base values were employed in DEM model. As seen in the figure, the normalized MFR fluctuates fiercely with Q_{vc} of 0.133, meaning that mass flow of particles is unsteady and then the layered powder bed will be uneven although the layering height and layering speed are constant during the layering. This is different from the flow of liquid, due to the discontinuous nature of powder particles [26,40]. The average value of normalized MFR, $\overline{Q}$, is just 0.381, indicating that the layered powder bed is far from the state of full density where $\overline{Q} = 1$.

3.3. Effects of cohesion force, particle properties and processing condition

The effects of cohesion force, particle properties and processing conditions on the flowing behavior of powder-layering will be discussed in terms of DRA and MFR.

3.3.1. Effect of cohesion force

As cohesion force increases the resistance which restricts the relative motion between powder particles [35], it will reduce the fluidity of powder particles, and hence the continuity and stability of the powder flow become worse. It is a general rule in application occasions such as particle discharging [23], grinding [20] and particle mixing [21]. Then, this is also the case in the powder-layering process of SLM.

Fig. 8 shows the effects of cohesion force on the flow behavior of

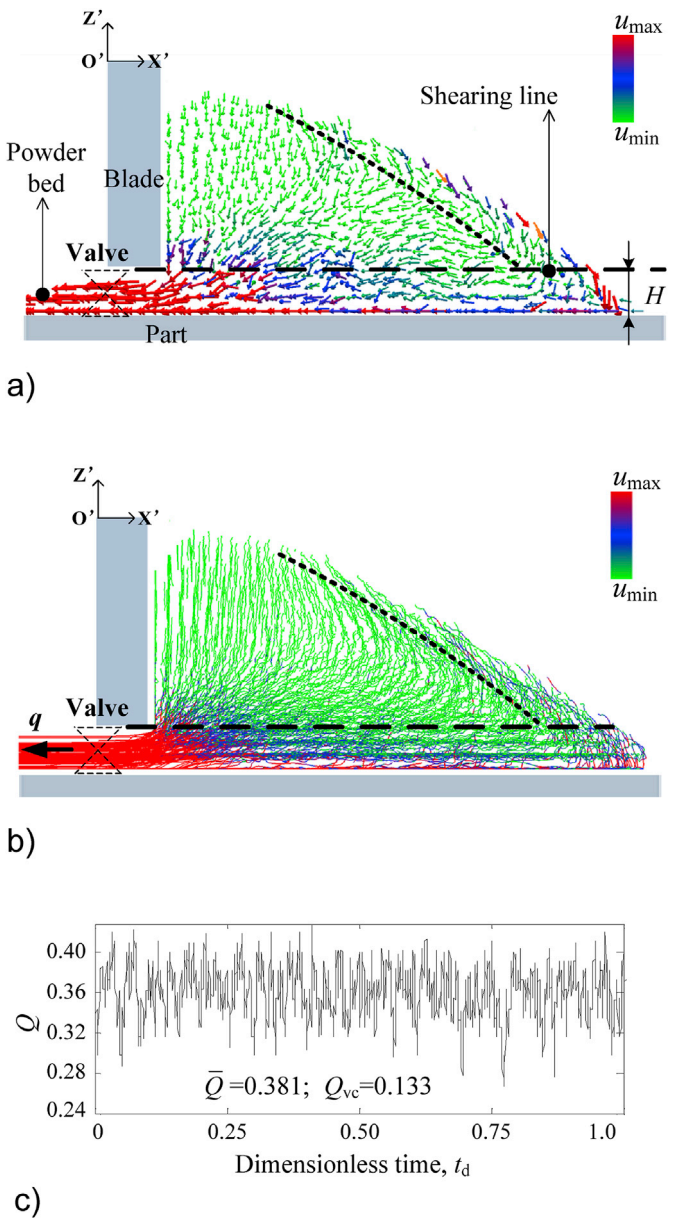

Fig. 7. DEM results in the layering-stage using variables with the base values: (a) velocity field of powder particles in the coordinate system O′-X′Y′Z′ at the time of $t_d = 0.5$; (b) trajectory of powder particles in the coordinate system O′-X′Y′Z′; and (c) evolution of normalized MFR, Q, with dimensionless time t_d, where $\overline{Q}$ and Q_{vc} are the average value and variation coefficient of Q, respectively.

powder-layering, where the surface energy density γ of 0, 1.7, 6.8 and 17 mJ/m^2 were used in the DEM model, corresponding to the bonding-number K of 0, 10, 40, and 100 from Eq. (7), respectively. As shown in Fig. 8a, when the cohesion force increases with the surface energy density which increases from 0 to 17 mJ/m^2, the fluidity of powder is reduced greatly, making the slope of the powder pile steeper. Furthermore, at the high cohesion force of $\gamma = 17$ mJ/m^2, the particle even bond together during the layering, which is unfavorable for powder-layering. The value of DAR, which increases from 28.6° to 82.6°, makes apt description about this phenomenon.

As the fluidity of powder is decreased by the enhanced cohesion force, the continuity and stability of the powder flow during layering will be reduced, which makes the quality of the layered powder bed worse. Fig. 8b shows the layered powder bed at particle scale, together with the average value of normalized MFR, $\overline{Q}$, and the variation coefficient of normalized MFR, Q_{vc}. Note that the sample of the powder bed was extracted from the center of the layering zone, and the position of particles in Z direction, h_z, was marked to facilitate the visualization of the state of powder bed. As shown, when the surface energy density increases from 0 to 17 mJ/m^2, the value of $\overline{Q}$ is decreased by about sixty times (from 0.381 to 0.058). It indicates that the packing density of the layered powder bed is reduced greatly, which can also be recognized qualitatively by the space between the shearing line and the surface of the powder bed. Meanwhile, the powder flow fluctuates more fiercely with Q_{vc} increased about ten times (from 0.133 to 1.233). Then, the powder bed goes to a worse condition of uniformity. As seen in the figure, the cavities in the powder bed become more and bigger, or even crack the powder bed into pieces completely. Above all, the cohesion force will reduce the powder fluidity, and then the continuity and stability of the powder flow during layering, which decreases the quality of the powder bed such as packing density and uniformity.

3.3.2. *Effect of particle properties*

Essentially, all the properties of particle listed in Table 2 can affect the flow behavior of powder-layering. However, in practical applications, some parameters are difficult or even impossible to adjust for a given kind of powder material such as particle density, Poisson ratio, and Young's modulus. Therefore, the discussion below is just focused on the variables which have significant effects on the powder flow and are convenient to adjust in practice, such as rolling friction coefficient μ_r, sliding friction coefficient μ_s, and particle radius R. And for simplicity, the visualization of the powder pile and layered powder bed will not be presented in details.

Fig. 9 shows the effects of rolling friction coefficient on the DRA and normalized MFR for different sliding friction coefficients. As shown in Fig. 9, for a given sliding friction coefficient, increasing the rolling friction coefficient leads to a larger $\overline{\alpha}$, with the decreased $\overline{Q}$ and increased Q_{vc}. This is because a larger rolling friction coefficient means an enhanced resistance force to the rotational motion between particles, which makes the rotation of particles more difficult [21] and hence reduce the fluidity of the powder during layering. Then, the powder particles during layering will form a pile of high potential, appearing in a larger DRA. The continuity and stability of powder flow gets worse with the decreasing of powder fluidity naturally. And moreover, the contact force network between powder particles will be strengthened by enhanced rolling resistance force, making its breaking more difficult and discontinuous [30,43]. Therefore, the MFR of the powder flow gets a smaller value of $\overline{Q}$ and a bigger value of Q_{vc}. This will decrease the packing density and uniformity of the layered powder bed and is unfavorable for the powder-layering.

Similarly, sliding friction governs the translational motion of particles. A larger sliding friction coefficient can tolerate a larger magnitude of the elastic deformation in the tangential direction of contacts between particles [45]. It gives a stronger resistance force to the translational motion of particle and strengthens the contact force network between particles, which will reduce the powder fluidity, and hence the stability of powder flow during layering. Therefore, the effect of sliding friction coefficient is similar to that of rolling friction coefficient, i.e., a larger sliding friction coefficient leads to an increased DRA, with the decreased $\overline{Q}$ and increased Q_{vc}. This is indeed the case as illustrated in Fig. 10.

Rotation and translation are the main motions of individual powder particles. The rolling and sliding frictions provide an effective mechanism to control the two motions and largely determine the fluidity of powder particles. In practical applications of SLM, the particles used for powder-layering should have the property of good spherical shape and surface integrity, which can decrease the rolling and sliding friction coefficients. Such particles, as discussed, have better fluidity during layering and then a denser and more homogeneous powder bed can be layered. And this is indeed the case which has been qualitatively observed in powder-layering [14,15]. However, even for $\mu_r = 0$ or $\mu_s = 0$,

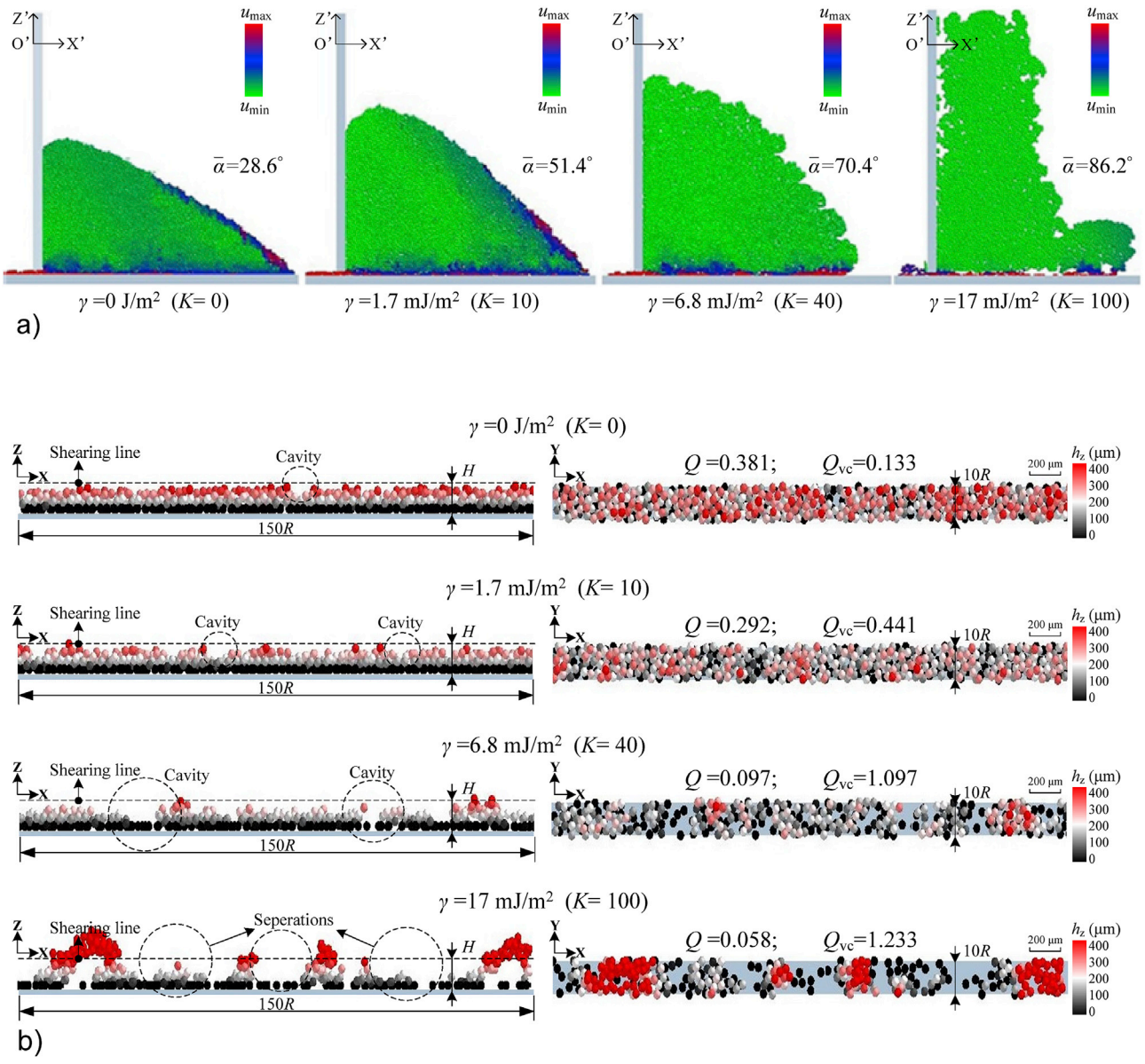

Fig. 8. DEM results of powder-layering with surface energy density γ of 0, 1.7, 6.8 and 17 mJ/m^2, respectively: (a) profiles of powder pile, together with the DRA $\bar{\alpha}$; (b) parts of the layered powder bed at particle scale, together with the average value of normalized MFR, $\overline{Q}$, and the variation coefficient of normalized MFR, Q_{vc}.

the values of $\overline{Q}$ is no more than 0.6 and Q_{vc} is no less than 0.08 (see Figs. 9 and 10, respectively). It means that the idea state of powder-layering, i.e.,$\overline{Q}$ = 1 and Q_{vc} = 0, can not be achieved even though the powder particle has the perfect shape quality and surface integrity.

The effect of particle size on the flow behavior of particulate system has been studied by a number of investigators in conditions such as granule piling [45], and discharging [22–24], where the particles are in millimeter level and thus the Fan der Waals' force can be ignored [34,35]. A general conclusion is that a bigger particle size makes disadvantage to the fluidity of powder particles, and thus to the continuity and stability of the powder flow. This law has also been observed in the present study without considering the cohesion force in DEM model (γ = 0 J/m^2), illustrated in Fig. 11. As the particle radius increases from 30 to 135 μm, the value of $\bar{\alpha}$ increases about 3° (Fig. 10a), indicating that the powder fluidity is reduced. Then, $\overline{Q}$ decreases from 0.43 to 0.34 and Q_{vc} increases from 0.127 to 0.138 (Fig. 10b), owing to the decrease of continuity and stability of the powder flow. Based on these results, using smaller particles can improve the powder fluidity and hence benefit the packing density and uniformity of the powder bed. However, it should be noted that the cohesion force was not involved in Fig. 11, i.e., it is the pure effect of the particle size. However, the Fan der Waal' force is considerable for fine powder used in SLM [14] and closely related to the particle size (see Eq. (6) and Eq. (7)), which might change the relationship between the particle size and the powder flow.

Fig. 12 shows the relationship between the particle radius varying from 9 to 130 μm and the flow behavior of powder during layering, where the Fan der Waal' force was involved in the DEM model (the base value of surface energy density γ was used) and presented in terms of the bounding-number K. The value of Fan der Waal' force decreases with the decreasing of particle radius (see Eq. (6)). However, the bounding number, according to Eq. (7), is inversely proportion to the square of particle radius R^2, meaning that the weight of Fan der Waal' force actually increases with the decreasing of particle size. As plotted in Fig. 12a, when R decreases from 130 to 9 μm, the bonding-number K increases from 0.1 to 20. And similar to the results in Fig. 8 which has just been discussed, the fluidity of powder during layering will be reduced.

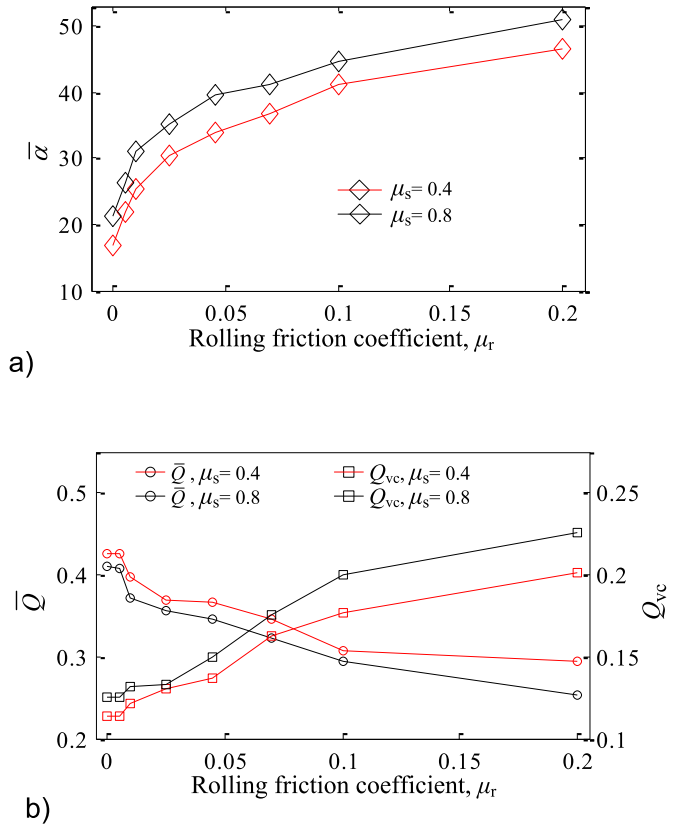

Fig. 9. (a) DRA, $\overline{\alpha}$; and (b) average value of normalized MFR, $\overline{Q}$, and variation coefficient of normalized MFR, Q_{vc}, as function of rolling friction coefficient μ_r. The sliding coefficients μ_s of 0.4 and 0.8 are employed, respectively.

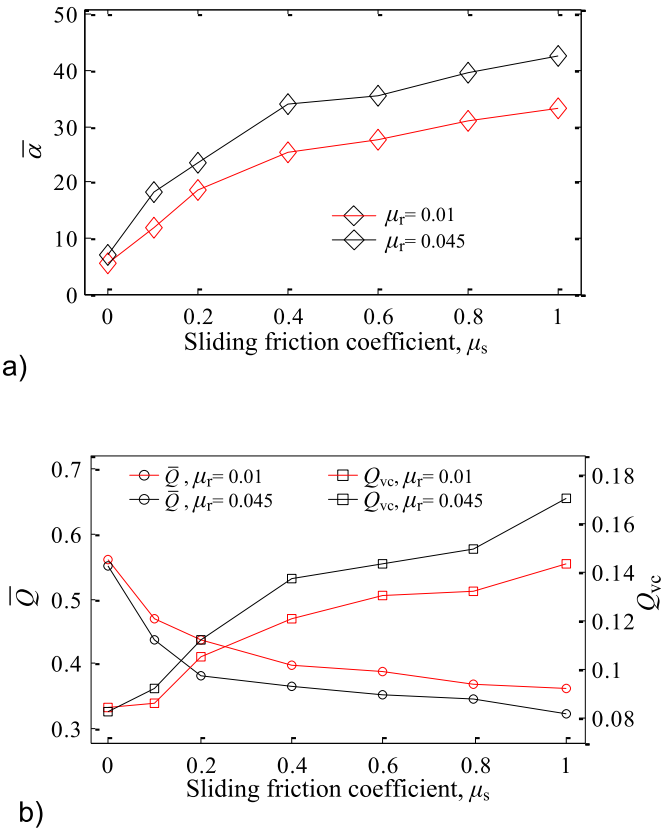

Fig. 10. (a) DRA, $\overline{\alpha}$; and (b) average value of normalized MFR, $\overline{Q}$, and variation coefficient of normalized MFR, Q_{vc}, as function of sliding friction coefficient μ_s. The rolling coefficients μ_r of 0.01 and 0.045 are employed, respectively.

Therefore, the DRA is increased by more than one time, as shown in Fig. 12b. Meanwhile, $\overline{Q}$ is about four times lower and Q_{vc} is nearly increased by nine times, as shown in Fig. 12c. It means that the quality of layered powder bed becomes worse with a reduced packing density and uniformity.

However, an interesting observation from Fig. 12b and c is that the fluidity of powder can be improved slightly when K increases in the range of $K < 3$ (i.e., R decreases in the range of $R > 21.8$ μm). As just discussed in Fig. 11, decreasing the particle radius can benefit the fluidity of powder, where the Fan der Waal' force between particles was not considered. So, the possible explanation for this observation is that, in the range of $R > 21.8$ μm (i.e., $K < 3$), the pure effect of particle size is strong and overwhelms that of Fan der Waal' force. Then, decreasing the particle radius can make the powder fluidity better. However, when the particle size decreases to the range of $R < 21.8$ μm (i.e., $K > 3$), the effect of particle size is surpassed and overwhelmed by that of Fan der Waal' force, and thus the fluidity of powder becomes worse. This can also be validated well by the visual powder profiles from simulations and experiments shown in Fig. 5. Therefore, it is inappropriate to improve the powder fluidity by decreasing the particle size without limit. Actually, a common phenomenon in practical SLM is that it is difficult to layer powder particles which are too fine [7,9]. For the 316L powder considered in this study, particle with radius no less than 21.8 μm will be the best choice for powder-layering.

3.3.3. *Effect of processing condition*

The layering speed V and height H are two major processing parameters which are adjustable during powder-layering. Fig. 13 shows the variations of $\overline{\alpha}$, $\overline{Q}$, and Q_{vc} with V and H respectively, where the layering height is normalized by the particle diameter $2R$. As shown in Fig. 13a, the effects of V and H on the DRA $\overline{\alpha}$ are negligible. This is because the profile of powder pile in a quasi-equilibrium state is governed by the acting forces between particles such as friction forces and cohesion forces [40,45]. These forces, as discussed above, are mainly determined by the particle properties related to the powder fluidity, rather than outside conditions such as V and H. Inertia force of particles can be affected by outside conditions [20,26], which might change the equilibrium of the powder pile. However, as the moving speed of the powder pile (i.e., the layering speed) is constant during layering, the variation of inertia force on the powder can be ignorable, and thus the equilibrium of the powder pile will not be affected by the outside conditions.

However, as shown in Fig. 13b, either increasing the layering speed or decreasing the layering height can make the value of $\overline{Q}$ smaller and Q_{vc} larger, which is unfavorable for the packing density and uniformity of the layered powder bed. For particulate system, its bulk volume will dilate during moving, and this dilation goes more intensely with the increasing of moving speed [21,44,47]. Therefore, when the layering speed V increases, the speed of particles crossing the valve (see Fig. 7a) will be increased, which enhances the dilation of these particles, making the particle flow looser and more discontinuous, with a smaller $\overline{Q}$ and larger Q_{vc}. In practical applications, it will be a tradeoff between the production efficiency and the quality of the powder bed when determining the layering speed. The effect of layering height H is similar to the situation of particle flow within a hopper [22–24]. The smaller the layering height, the easier it is to form local "force arches [42,45,46]" between powder particles, which will retard or even stop the particle flow at the valve. Naturally, the continuity and stability of powder flow are reduced, with a smaller $\overline{Q}$ and larger Q_{vc}. Instead, such "force arches" vanish gradually with the increasing of layering height, which will benefit the particle flow at the valve and thus improve the quality of layered powder bed.

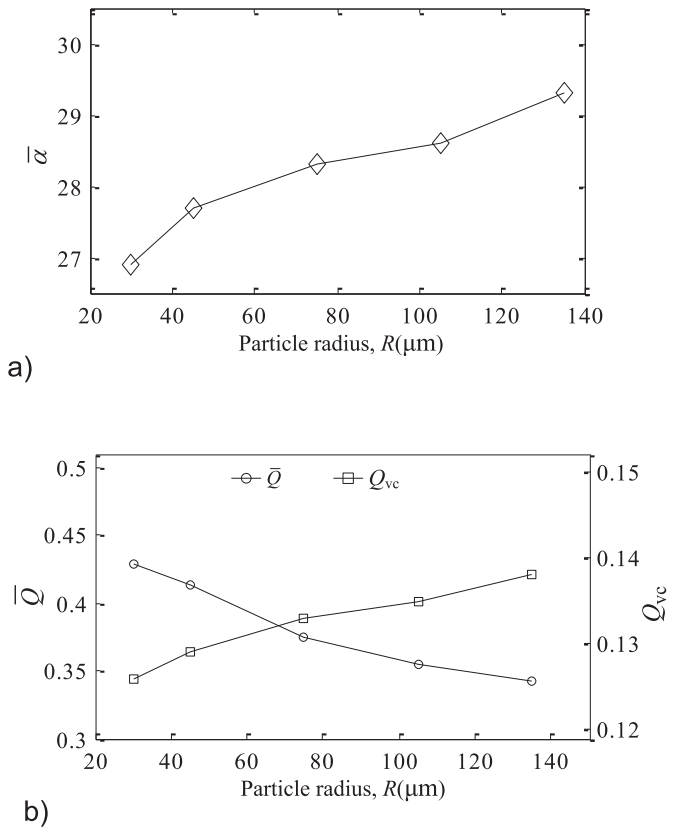

Fig. 11. (a) DRA, $\overline{\alpha}$; and (b) average value of normalized MFR, $\overline{Q}$, and variation coefficient of normalized MFR, Q_{vc}, as function of particle radius R.

Therefore, in practice, even without considering about the production efficiency [11,15], it is inappropriate to make the powder bed too thin. However, there is a limit for increasing the layering height to improve the quality of layered powder bed. In the condition of this study, as shown in Fig. 13b, the value of $\overline{Q}$ and Q_{vc} is no longer sensitive to the normalized layering height which is greater than four.

4. Conclusions

Numerical model based on discrete element method has been carried out to study the flow behavior of powder-layering, which is a necessary process of the additive manufacturing such as SLM. The powder-layering is divided into two stages: the collecting-stage and the layering-stage. The focus is given to the layering-stage related to the quality of the layered powder bed. Then, dynamic repose angle (DRA) and mass flow rate (MFR) are defined and used to make quantitative analysis on the powder flow at particulate scale, where MFR is normalized and presented in terms of its average value $\overline{Q}$ and variation coefficient Q_{vc}, respectively. The major findings are summarized as follows:

(1) The present DEM results are in good agreement with the experimental ones under comparable conditions in terms of the repose angle of powder pile during layering, confirming that the DEM method is an effective numerical technique for the investigation of powder-layering.
(2) With the decrease of either rolling friction coefficient or sliding friction coefficient between particles, the fluidity of powder during layering is improved, i.e., the DRA decreases. And then, the continuity and stability of powder flow during layering become better, i.e., the corresponding $\overline{Q}$ increases and Q_{vc} decreases. This can enhance the quality (the packing density and uniformity) of the layered powder bed.

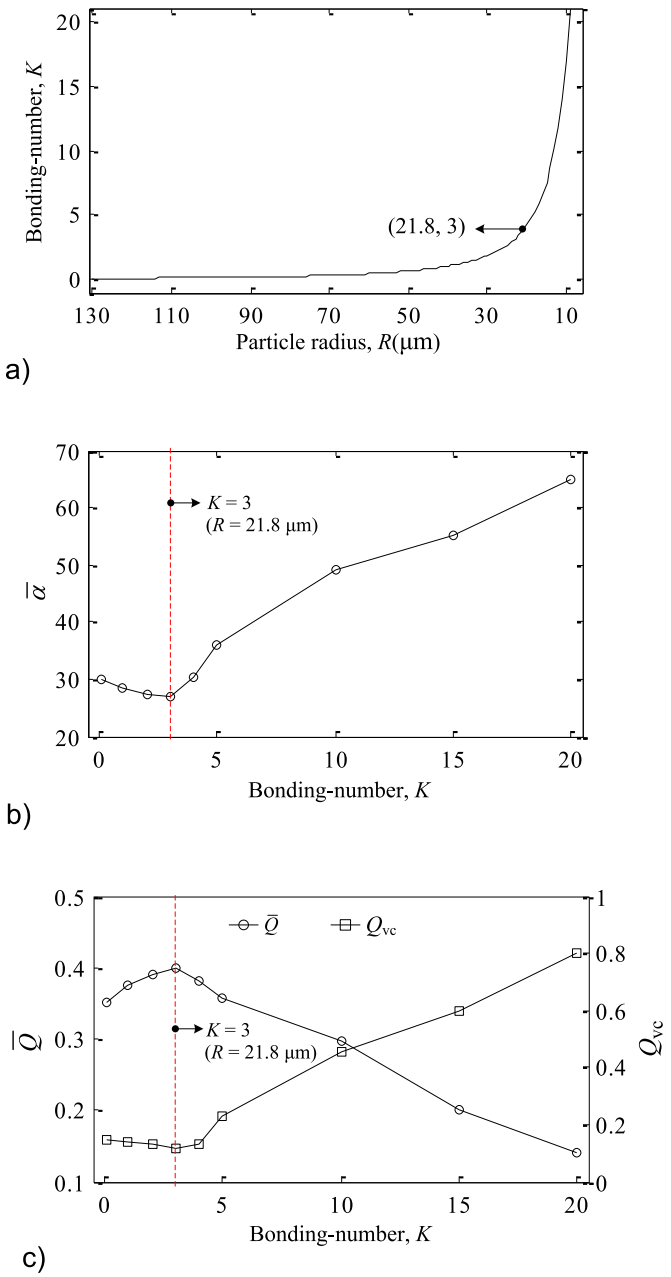

Fig. 12. (a) Bounding-number K as function of particle radius R; (b) DRA, $\overline{\alpha}$; and (c) average value of normalized MFR, $\overline{Q}$, and variation coefficient of normalized MFR, Q_{vc}, as function of bounding-number K.

(3) When the particle radius R decreases over the range of $R > 21.8$ μm, the fluidity of powder is improved, which benefits the quality of powder bed. However, in the range of $R < 21.8$ μm, the weight of Van der Waals' force rises and dominates owing to the decreasing of particle radius. This will make the powder fluidity worse and thus reduce the quality of layered powder bed.
(4) The effects of the layering speed and layering height on the fluidity of powder (the DRA) is ignorable. However, a larger layering speed can enhance the dilation of moving particles, and a smaller layering height is more likely to form local force arches between particles. These will damage the continuity and stability of the powder flow during layering, leading to a decreased $\overline{Q}$ and increased Q_{vc}. This is not beneficial for improving the packing density or uniformity of the layered powder bed.

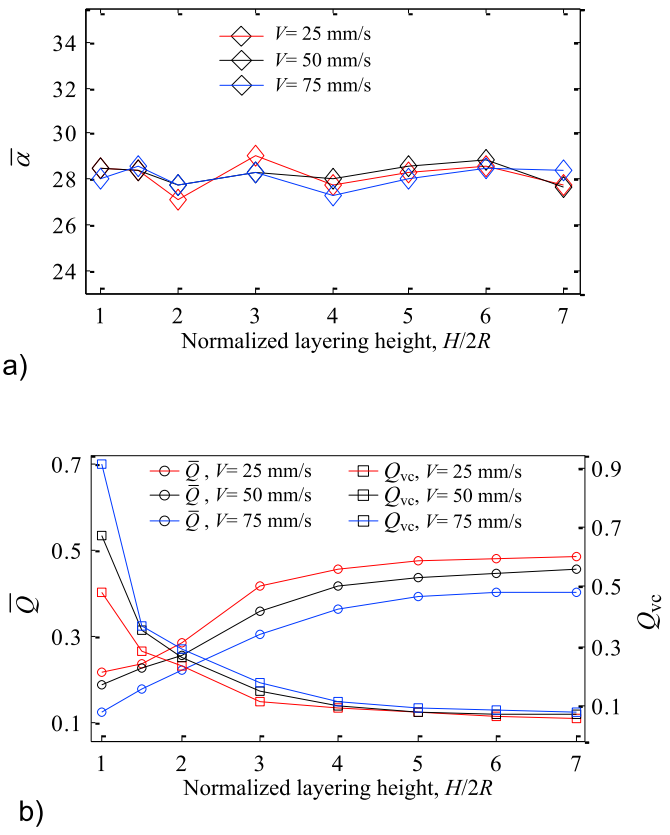

Fig. 13. (a) DRA, $\overline{\alpha}$; and (b) average value of normalized MFR, $\overline{Q}$, and variation coefficient of normalized MFR, Q_{vc}, as function of the layering height H which is normalized by particle diameter. The layering speed V is set to 25, 50, and 75 mm/s, respectively.

The flowing behavior of powder particles during layering, as far as we know, has never been quantitatively investigated at particle scale before. This study gives an understanding on the flow dynamics of powder-layering, and is helpful for improving the quality of layered powder bed in additive manufacturing such as SLM.

Acknowledgments

Authors are very grateful to the Foundation from China and the European Union: Horrizon 2020 “Efficient Manufacturing for Aerospace Components Using Additive Manufacturing, Net Shape HIP and Investment Casting (Grant No.: MJ-2015-H-G-104) ”; National Natural Science Foundation of China (Grant No.: 51705170); Academic Frontier Youth Team of Huazhong University of Science and Technology (HUST) and Fundamental Research Funds for the Central Universities (Grant No.: 2015ZDTD028); Hubei Science and Technology Support Program (Grant No. 2014BAA017) and Wuhan Key Technology Breakthrough Project (Grant No.: 201501020201008).

References

[1] M. Xia, D. Gu, G. Yu, D. Dai, H. Chen, Q. Shi, Porosity evolution and its thermodynamic mechanism of randomly packed powder-bed during selective laser melting of Inconel 718 alloy, Int. J. Mach. Tools Manuf. 116 (2017) 96–106.
[2] M. Matsumoto, M. Shiomi, K. Osakada, F. Abe, Finite element analysis of single layer forming on metallic powder bed in rapid prototyping by selective laser processing, Int. J. Mach. Tools Manuf. 42 (1) (2002) 61–67.
[3] S.A. Khairallah, A.T. Anderson, A. Rubenchik, W.E. King, Laser powder-bed fusion additive manufacturing: physics of complex melt flow and formation mechanisms of pores, spatter, and denudation zones, Acta Mater. 108 (2016) 36–45.
[4] D.D. Gu, W. Meiners, K. Wissenbach, R. Poprawe, Laser additive manufacturing of metallic components: materials, processes and mechanisms, Int. Mater. Rev. 57 (3) (2012) 133–164.
[5] L.C. Zhang, H. Attar, M. Calin, J. Eckert, Review on manufacture by selective laser melting and properties of titanium based materials for biomedical applications, Mater. Technol. 31 (2016) 66–76.
[6] F.J. Gutler, M. Karg, K.H. Leitz, M. Schmidt, Simulation of laser beam melting of steel powders using the three-dimensional volume of fluid method, Phys. Procedia 41 (2013) 881–886.
[7] Y.S. Lee, W. Zhang, Modeling of heat transfer, fluid flow and solidification microstructure of nickel-base superalloy fabricated by laser powder bed fusion, Addit. Manuf. 12 (2016) 178–188.
[8] S.A. Khairallah, A. Anderson, Mesoscopic simulation model of selective laser melting of stainless steel powder, J. Mater. Process. Technol. 214 (11) (2014) 2627–2636.
[9] S. Ziegelmeier, P. Christou, F. Wöllecke, C. Tuck, R. Goodridge, R. Hague, E. Krampe, E. Wintermantel, An experimental study into the effects of bulk and flow behaviour of laser sintering polymer powders on resulting part properties, J. Mater. Process. Technol. 215 (2015) 239–250.
[10] M.J. Matthews, G. Guss, S.A. Khairallah, A.M. Rubenchik, P.J. Depond, W.E. King, Denudation of metal powder layers in laser powder bed fusion processes, Acta Mater. 114 (2016) 33–42.
[11] M. Vaezi, C.K. Chua, Effects of layer thickness and binder saturation level parameters on 3D printing process, Int. J. Adv. Manuf. Technol. 53 (2011) 275–284.
[12] E.C. Santos, M. Shiomi, K. Osakada, T. Laoui, Rapid manufacturing of metal components by laser forming, Int. J. Mach. Tools Manuf. 46 (12) (2006) 1459–1468.
[13] G. Marchelli, R. Prabhakar, D. Storti, M. Ganter, The guide to glass 3D printing: developments, methods, diagnostics and results, Rapid Prototyp. J. 17 (3) (2011) 187–194.
[14] K. Lu, W.T. Reynolds, 3DP process for fine mesh structure printing, Powder Technol. 187 (1) (2008) 11–18.
[15] S. Cao, Y. Qiu, X.F. Wei, H.H. Zhang, Experimental and theoretical investigation on ultra-thin powder layering in three dimensional printing (3DP) by a novel double-smoothing mechanism, J. Mater. Process. Technol. 220 (2015) 231–242.
[16] Z. Xiang, M. Yin, Z. Deng, X. Mei, G. Yin, Simulation of forming process of powder bed for additive manufacturing, J. Manuf. Sci. Eng. 138 (8) (2016), 081002.
[17] P.A. Cundall, O.D. Strack, A discrete numerical model for granular assemblies, Geotechnique 29 (1) (1979) 47–65.
[18] L.A.M. Camones, E. do Amaral Vargas, R.P. de Figueiredo, R.Q. Velloso, Application of the discrete element method for modeling of rock crack propagation and coalescence in the step-path failure mechanism, Eng. Geol. 153 (2013) 80–94.
[19] B. Alchikh-Sulaiman, F. Ein-Mozaffari, A. Lohi, Evaluation of poly-disperse solid particles mixing in a slant cone mixer using discrete element method, Chem. Eng. Res. Des. 96 (2015) 196–213.
[20] P.W. Cleary, A multiscale method for including fine particle effects in DEM models of grinding mills, Miner. Eng. 84 (2015) 88–99.
[21] K.F. Lee, M. Dosta, A.D. McGuire, S. Mosbach, W. Wagner, S. Heinrich, M. Kraft, Development of a multi-compartment population balance model for high-shear wet granulation with discrete element method, Comput. Chem. Eng. 99 (2017) 171–184.
[22] S.D. Liu, Z.Y. Zhou, R.P. Zou, D. Pinson, A.B. Yu, Flow characteristics and discharge rate of ellipsoidal particles in a flat bottom hopper, Powder Technol. 253 (2014) 70–79.
[23] G. Gutiérrez, C. Colonnello, P. Boltenhagen, J.R. Darias, R. Peralta-Fabi, F. Brau, E. Clément, Silo collapse under granular discharge, Phys. Rev. Lett. 114 (1) (2015), 018001.
[24] Q.J. Zheng, A.B. Yu, Finite element investigation of the flow and stress patterns in conical hopper during discharge, Chem. Eng. Sci. 129 (2015) 49–57.
[25] E. Alizadeh, F. Bertrand, J. Chaouki, Comparison of DEM results and Lagrangian experimental data for the flow and mixing of granules in a rotating drum, AIChE J. 60 (1) (2014) 60–75.
[26] Y. Guo, J.S. Curtis, Discrete element method simulations for complex granular flows, Annu. Rev. Fluid Mech. 47 (2015) 21–46.
[27] A. Hassanpour, M. Pasha, L. Susana, N. Rahmanian, A.C. Santomaso, M. Ghadiri, Analysis of seeded granulation in high shear granulators by discrete element method, Powder Technol. 238 (2013) 50–55.
[28] E.J. Parteli, T. Pöschel, Particle-based simulation of powder application in additive manufacturing, Powder Technol. 288 (2016) 96–102.
[29] J.C. Steuben, A.P. Iliopoulos, J.G. Michopoulos, Discrete element modeling of particle-based additive manufacturing processes, Comput. Methods Appl. Mech. Eng. 305 (2016) 537–561.
[30] H. Chen, Y.L. Liu, X.Q. Zhao, Y.G. Xiao, Y. Liu, Numerical investigation on angle of repose and force network from granular pile in variable gravitational environments, Powder Technol. 283 (2015) 607–617.
[31] P.A. Langston, M.A. Al-Awamleh, F.Y. Fraige, B.N. Asmar, Distinct element modelling of non-spherical frictionless particle flow, Chem. Eng. Sci. 59 (2) (2004) 425–435.
[32] Y. Tsuji, T. Tanaka, T. Ishida, Lagrangian numerical simulation of plug flow of cohesionless particles in a horizontal pipe, Powder Technol. 71 (3) (1992) 239–250.
[33] A. Di Renzo, F.P. Di Maio, Comparison of contact-force models for the simulation of collisions in DEM-based granular flow codes, Chem. Eng. Sci. 59 (3) (2004) 525–541.
[34] K.L. Johnson, I. Sridhar, Adhesion between a spherical indenter and an elastic solid with a compliant elastic coating, J. Phys. D Appl. Phys. 34 (5) (2001) 683.
[35] E. Barthel, Adhesive elastic contacts: JKR and more, J. Phys. D Appl. Phys. 41 (16) (2008), 163001.

[36] F.A. Gilabert, J.N. Roux, A. Castellanos, Computer simulation of model cohesive powders: influence of assembling procedure and contact laws on low consolidation states, Phys. Rev. E 75 (1) (2007), 011303.
[37] C. O'Sullivan, J.D. Bray, Selecting a suitable time step for discrete element simulations that use the central difference time integration scheme, Eng. Comput. 21 (2004) 278–303.
[38] K.J. Hanley, C. O'Sullivan, Analytical study of the accuracy of discrete element simulations, Int. J. Numer. Methods Eng. 109 (1) (2017) 29–51.
[39] M. Alonso, M. Satoh, K. Miyanami, Optimum combination of size ratio, density ratio and concentration to minimize free surface segregation, Powder Technol. 68 (2) (1991) 145–152.
[40] Y.C. Zhou, B.H. Xu, A.B. Yu, P. Zulli, Numerical investigation of the angle of repose of monosized spheres, Phys. Rev. E 64 (2001), 021301.
[41] C.J. Coetzee, Review: calibration of the discrete element method, Powder Technol. 310 (2017) 104–142.
[42] F. Radjai, M. Jean, J.J. Moreau, S. Roux, Force distributions in dense two-dimensional granular systems, Phys. Rev. Lett. 77 (2) (1996) 273–277.
[43] B.P. Tighe, A.R.T. van Eerd, T.J.H. Vlugt, Entropy maximization in the force network ensemble for granular solids, Phys. Rev. Lett. 100 (2008), 238001.
[44] P.S. Goswami, V. Kumaran, Particle dynamics in the channel flow of a turbulent particle–gas suspension at high Stokes number. Part 1. DNS and fluctuating force model, J. Fluid Mech. 687 (2011) 1–40.
[45] Y.C. Zhou, B.H. Xu, A.B. Yu, P. Zulli, Numerical investigation of the angle of repose of monosized spheres, Phys. Rev. E 64 (2) (2001), 021301.
[46] T.S. Majmudar, R.P. Behringer, Contact force measurements and stress-induced anisotropy in granular materials, Nature 435 (7045) (2005) 1079–1082.
[47] A. Castellanos, J.M. Valverde, A.T. Pérez, A. Ramos, P.K. Watson, Flow regimes in fine cohesive powders, Phys. Rev. Lett. 82 (6) (1999) 1156.